THE JOURNAL OF PHYSICAL CHEMISTRY B
A JOURNAL OF THE AMERICAN CHEMICAL SOCIETY

pubs.acs.org/JPCB

Article

Mechanistic Picture for Chemomechanical Coupling in a Bacterial Proton-Coupled Oligopeptide Transporter from Streptococcus Thermophilus

Kalyan Immadisetty and Mahmoud Moradi*

Cite This: *J. Phys. Chem. B* 2021, 125, 9738−9750

Read Online

ACCESS | Metrics & More | Article Recommendations | Supporting Information

ABSTRACT: Proton-coupled oligopeptide transporters (POTs) use the proton electrochemical gradient to transport peptides across the cell membrane. Despite the significant biological and biomedical relevance of these proteins, a detailed mechanistic picture for chemomechanical couplings involved in substrate/proton transport and protein structural changes is missing. Therefore, we performed microsecond-level molecular dynamics simulations of bacterial POT $PepT_{St}$, which shares ∼80% sequence identity with the human POT, PepT1, in the substrate-binding region. Three different conformational states of $PepT_{St}$ were simulated, including (i) occluded, *apo*, (ii) inward-facing, *apo*, and (iii) inward-facing$_{occluded}$, Leu−Ala bound. We propose that the interaction of R33 with E299 and E300 acts as a conformational switch (i.e., to trigger the conformational change from an inward- to outward-facing state) in the substrate transport. Additionally, we propose that E299 and E400 disengage from interacting with the substrate either through protonation or through coordination with a cation for the substrate to get transported. This study provides clues to understand the chemomechanical couplings in POTs and paves the way to decipher the molecular-level underpinnings of the structure−function relationship in this important family of transporters.

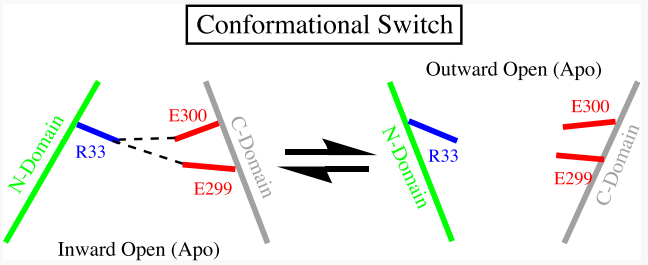

INTRODUCTION

Proton-coupled oligopeptide transporters (POTs) are membrane proteins present in the brush borders of the kidneys and the small intestine.[1] POTs belong to the major facilitator super (MFS) family, and important features of this family of proteins are substrate promiscuity and the presence of multiple substrate-binding regions,[2] which are thought to be responsible for the ability of substrates/peptides to bind in multiple orientations[1,3,4] and with varying stoichiometry.[5] This feature of POTs is of great interest due to its biomedical relevance.[6−8] Human POTs (PepT1 and PepT2) absorb and retain a wide range of di- and tripeptides and peptide-like compounds.[4,9] They also recognize and help improve the bioavailability of poorly absorbed peptide-like drug compounds such as β-lactam antibiotics,[10] angiotensin-converting enzyme inhibitors, and antiviral prodrugs.[11−15] Despite their biomedical relevance, several aspects of POTs are still debated, mainly substrate/peptide binding and transport mechanism and proton modulation of this process. This is mainly due to the nonavailability of human POT (PepT1 and PepT2) crystal structures. However, crystal structures of several bacterial homologues of human POTs, such as $PepT_{So}$,[3,16] $PepT_{St}$,[17,18] $PepT_{So2}$,[7] and GkPOT,[19] are available.

It has been proposed that the POTs follow an alternating access mechanism[20] for transporting the substrates.[17] According to this mechanism, a POT has to undergo at least four major conformational changes for it to facilitate transport, mainly outward-facing (apo), occluded (substrate-bound), inward-facing (apo), and occluded (apo).[1,4] All the bacterial POT crystal structures reported to date are either occluded (OCC),[18] inward-facing$_{occluded}$(IF_{occ}), or inward-facing (IF) states;[3,7,16−18,21,22] an outward-facing (OF) state is not yet available. Even the MD studies that were reported earlier on POTs[19,23,24] failed to capture the fully open and stable OF conformation. Fowler et al. generated a $PepT_{So}$ model in an OF state through the repeat-swapping technique;[25,26] however, they were not able to validate it through th double electron−electron resonance experiments.[24]

$PepT_{St}$ is a bacterial POT symporter from *Streptococcus thermophilus*. Several studies have been carried out to investigate different aspects of $PepT_{St}$ through various experimental[5,18,22,24,27,28] and computational techniques,[24,28,29] including solving protein structures in various conformations,[17,18,22,27] understanding and proposing the functional mechanism,[4,17,24] identifying different substrate-binding sites

Received: May 4, 2021
Revised: July 22, 2021
Published: August 23, 2021

Table 1. Different Systems Simulated via MD in this Study

system	UP:E300	P:E300	P:E299	P:E400	P:E299,300	P:E299,400	P:E300,400	P:E299,300,400
occ(Apo)[a] (μs)	1	1						
IF(Apo)[b] (μs)	1	1						
IF_{occ}(LA)[c] (μs)	1	1	1	1	1	1	1	1

[a]Occluded $PepT_{St}$ in the apo form. [b]IF $PepT_{St}$ in the apo form. [c]IF_{occ} $PepT_{St}$ bound with the LA substrate. UP and P refer to deprotonated and protonated residues, respectively.

and multiple binding modes for the substrates,[4,5] multispecific substrate recognition pathways,[3,18] the mechanism of proton and peptide coupling,[28] different transport mechanisms for different POTs,[4,28] and binding of a range of substrates.[29] However, a study utilizing all available conformations of the $PepT_{St}$ is needed to gain a detailed atomistic level understanding of its transport mechanism, and the current availability of multiple conformations of $PepT_{St}$ provides a perfect opportunity.[17,18,22,27]

$PepT_{St}$ is the only POT symporter that has been crystallized in OCC, IF, and IF_{occ} conformational states.[17,18,22,27] Hence, in this study, we simulated all three available conformational states of $PepT_{St}$ via unbiased all-atom MD[30−33] with either E300 protonated or deprotonated. Additionally, we simulated IF_{occ} Leu−Ala (LA) in all possible protonation combinations of E299, E300, and E400 residues, which resulted in a total of eight substrate-bound systems (see Methods for more details). The LA substrate binds with millimolar affinity (≈0.56 mM) to $PepT_{St}$.[18] It was demonstrated that the three glutamates lining the substrate translocation path (i.e., E299, E300, and E400) are very important for the functioning of the $PepT_{St}$,[4,17,18] and E400, in particular, is conserved across all members of the family.

Overall, we simulated 12 different systems (see Table 1 for details), each for ≈1 μs (12 μs in total, and this is the highest simulation time for any POT reported thus far). We propose that (1) the R33−E299 and R33−E300 salt bridge interactions act as a molecular switch for the protein to undergo a complete conformational change from an IF side to an OF side, (2) deprotonation of E300 and, thus, the formation of the R33−E300 salt bridge is crucial for the protein to transform from an OF side to an occluded/IF side, (3) disengaging E299 and E400 from interacting with the LA substrate is the key step for it to get transported, (4) either protonation of E299 and/or E400 or coordination of E299 and E400 with sodium prevent these residues from engaging with the substrate and facilitate its transport, and (5) the C-domain is more dynamic than the N-domain, and the C-domain plays a key role in the transportation process, particularly transmembrane (TM) helices 7, 10, and 11.

METHODS

Twelve different $PepT_{St}$ systems (Table 1) were simulated via all-atom unbiased MD, each for 1 μs. Three different crystal structures of $PepT_{St}$ were utilized in this study: (a) $PepT_{St}$ in the IF state and complexed with HEPES (PDB: 6EIA), (2) $PepT_{St}$ in the IF_{occ} state and bound to the LA dipeptide (PDB: 5OXL), and (3) $PepT_{St}$ in the OCC state and bound with a phosphate ion in the substrate-binding site (PDB: 5OXP).[22] All the three crystal structures were downloaded from the protein data bank and processed using MOE software.[34] Crystal waters and other components except the dipeptide substrate were removed from the crystal structures, which resulted in one dipeptide bound $PepT_{St}$ in the IF_{occ} conformation, one $PepT_{St}$ in the IF(apo) conformation, and one $PepT_{St}$ in the OCC(apo) conformation. The missing residues in these three structures were modeled using MOE software and protonation states were assigned using the protonate 3D facility in MOE. These three $PepT_{St}$ systems were modeled with either E300 protonated [P:E300:I-F_{occ}(LA)] or deprotonated [UP:E300:IF_{occ}(LA)], resulting in six different systems. The substrate bound form was also modeled in six other protonation states: (1) E299 protonated [P:E299:IF_{occ}(LA)], (2) E400 protonated [P:E400:IF_{occ}(LA)], (3) E299 and E300 protonated [P:E299,300:IF_{occ}(LA)], (4) E299 and E400 protonated [P:E299,400:IF_{occ}(LA)], (5) E299 and E400 protonated [P:E299,400:IF_{occ}(LA)], and (6) E299, E300 and E400 protonated [P:E299,300,400:IF_{occ}(LA)]. The OPM web server was used to orient the protein in the membrane.[35] Further, all 12 systems were built for MD simulations using the CHARMM-GUI web server.[36] Each system consists of one $PepT_{St}$, ∼18,353 TIP3P waters,[37] ∼280 POPE lipids, and 0.15 M NaCl; and an additional dipeptide in the substrate-bound systems. The size of each system was ∼100 × 100 × 101 Å^3 and contains ∼97,500 atoms. Each system was first energy minimized via the conjugate gradient algorithm[38] for 10,000 steps and then relaxed in multiple steps (see ref 39 for details) for a total of ∼1.5 ns in an *NVT* ensemble. Fully unbiased simulations started from the relaxed models in an *NPT* ensemble, and data were collected every 0.5 ns for a total of 1 μs in each case. Because the relaxation step was short, we considered the first 200 ns of *NPT* equilibrium simulations as the "equilibration stage" and only used the last 800 ns of these simulations as "production runs". Simulations were conducted using NAMD 2.12[40] in periodic boundary conditions, and data analysis was conducted using various VMD plugins.[41] All components were modeled using the CHARMM36 all-atom additive force field.[42] A 2 fs time step was used and simulations were carried at 310 K using a Langevin integrator with a damping coefficient of γ = 0.5 ps^{-1} and pressure was maintained at 1 atm using the Nosé−Hoover Langevin piston method.[43,44] The nonbonded interaction cut-off distance was set to 10−12 Å, and the particle mesh Ewald method[45] was used to compute the long-range electrostatic interactions. We have used 24,000 data points (12 systems × 2 data points/ns × 1 μs = 24,000) for analysis in this work. PRODY software package[46] was used for principal component analysis (PCA).[47,48] The PCA was carried on an ensemble of DCD structures and 20 modes were generated.

RESULTS AND DISCUSSION

In this study, we investigated the impact of protonation/deprotonation of the three negatively charged residues (i.e., E299, E300, and E400) lining the peptide binding site on the structure and dynamics of the $PepT_{St}$ transporter in atomistic detail. Twelve different structures of $PepT_{St}$ in different protonation/deprotonation combinations of E299, E300, and E400 were simulated via all-atom MD. See the Methods

https://doi.org/10.1021/acs.jpcb.1c03982
J. Phys. Chem. B 2021, 125, 9738−9750

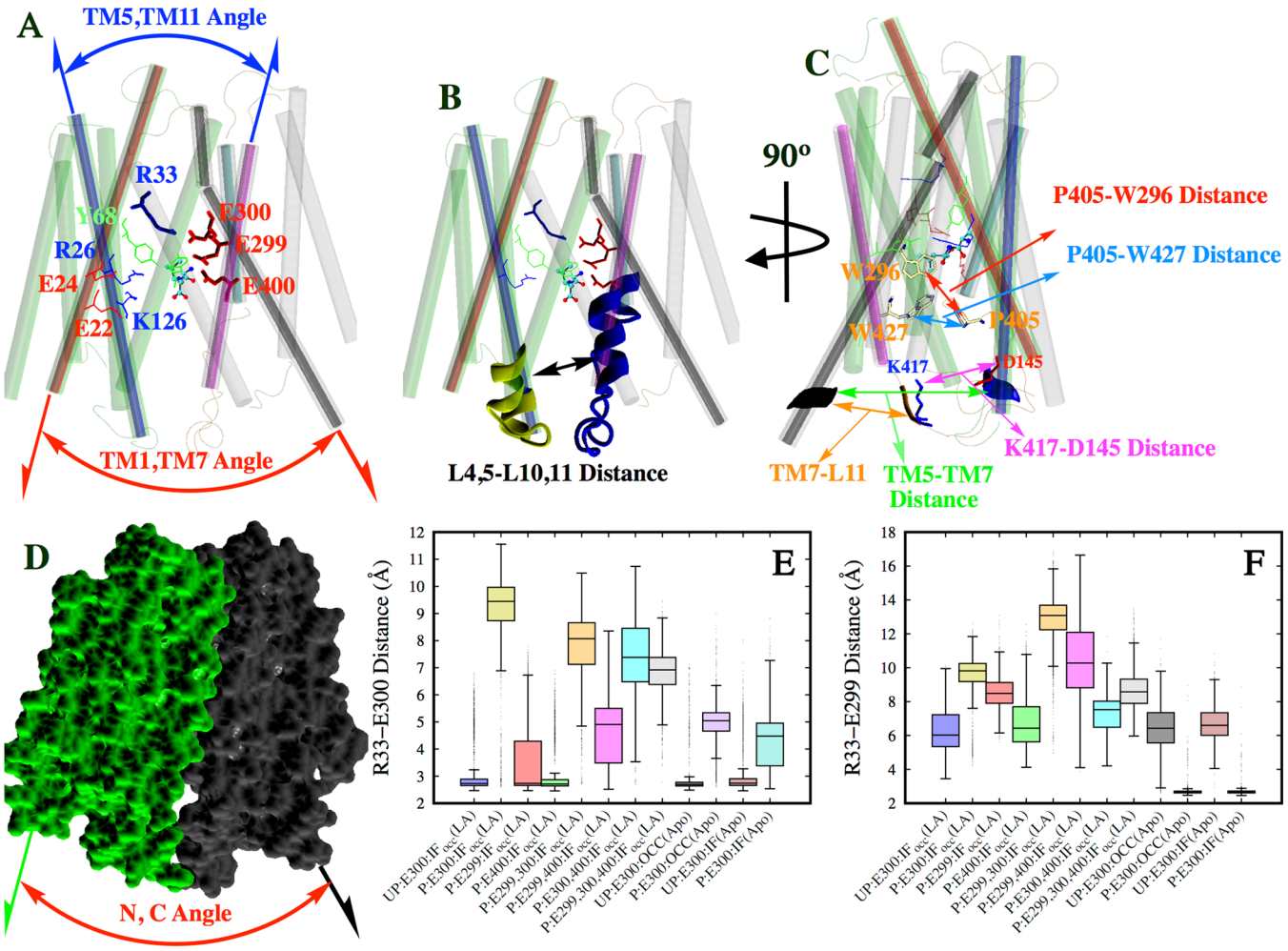

Figure 1. (A) $PepT_{St}$ comprises 14 TM helices; 12 are arranged in 2 bundles as N- (green, TMs 1−6) and C-domains (gray, TMs 7−12). The two other helices are not shown because their role in the functioning of the POTs is not yet established. Positive and negative residues are colored blue and red, respectively. The LA substrate is colored cyan and shown in ball and stick representation. Interhelical angles TM1 and TM7 (red) and TM5 and TM11 (blue) represent extracellular and intracellular gates, respectively, which are thought to control the substrate transport.[1,4] (B) Distance between $L_{4,5}$ and $L_{10,11}$. $L_{4,5}$ is the loop between the helices TM4 and TM5. $L_{10,11}$ is the loop between the helices TM10 and TM11. (C) Various other variables measured along the substrate translocation path. P405−W296 (red) is the distance between the residues P405 and W296, P405−W427 (blue) is the distance between the residues P405 and W427, K417−D145 (magenta) is the distance between the residues K417 and D145, TM7−L11 (orange) is the distance between the TM7 and loop L11, and TM5−TM7 (green) is the distance between the TM helices 5 and 7. Residues 280−281 (TM7) and 418−419 (L11) were considered for the TM7−L11 distance calculation. Residues 144−145 (TM5) and 280−281 (TM7) were considered for the TM5−TM7 distance calculation. (D) N-,C-interdomain angle. N- and C-terminal domains are colored green and black, respectively. The interdomain and interhelical angles were calculated as the angle between the third principal axes of the corresponding domains/helices. (E,F) Box plots of distances of R33−E300 (E) and R33−E299 (F) salt bridges. The boxes represent the 25th to 75th quartile, the horizontal line inside the box represents the median, whiskers represent the minima and maxima, and the outliers are shown as points above and below the whiskers. The salt bridges were calculated as the minimum distance between the two interacting residues. The presence of the LA substrate destabilized the R33−E300 salt bridge in all systems with the E300 deprotonated, whereas the absence of the substrate keeps this salt bridge intact. This salt bridge is lost in all the E300 deprotonated systems as expected, although, in the apo systems, this salt bridge distance is smaller compared to the substrate-bound systems. The R33−E299 salt bridge is absent in all other systems, with the exception of the P:E300:OCC(Apo) and P:E300:IF(Apo) systems. The last 800 ns of simulation data was utilized for the salt bridge box plot generation. Residues comprising TM helices and loops (L) are as follows: TM1: 13−46; TM2: 53−81; TM3: 83−104; TM4: 107−133; TM5: 142−173; TM6: 175−197; TMA: 213−242; TMB: 245−266; TM7: 282−312; TM8: 321−347; TM9: 354−383; TM10: 385−405; TM11: 424−446; TM12: 450−482; L1: 131−146; and L2: 400−430.

section for further details. Based on the 12 μs of MD simulation data that was generated, we studied various aspects including the interactions of R33 with E299/E300/E400, interactions of the LA substrate with E299/E300/E400, and the role of protonation/deprotonation of the residues E299/E300/E400 in the conformational dynamics of the protein and substrate translocation pathway. Additionally, we also propose favorable conditions for the substrate to get transported in the $PepT_{St}$. All these aspects are discussed below in detail.

R33−E300 and R33−E299 Salt Bridge Interactions Act as a Conformational Switch for $PepT_{St}$ to Transition from an IF(Apo) State to an OF(Apo) State. E300 belongs to TM7 and resides at the intersection of C- and N-domains. Studies reported that E300 plays a key role in the functional dynamics of the POT family of transporters by forming a salt

https://doi.org/10.1021/acs.jpcb.1c03982
J. Phys. Chem. B 2021, 125, 9738−9750

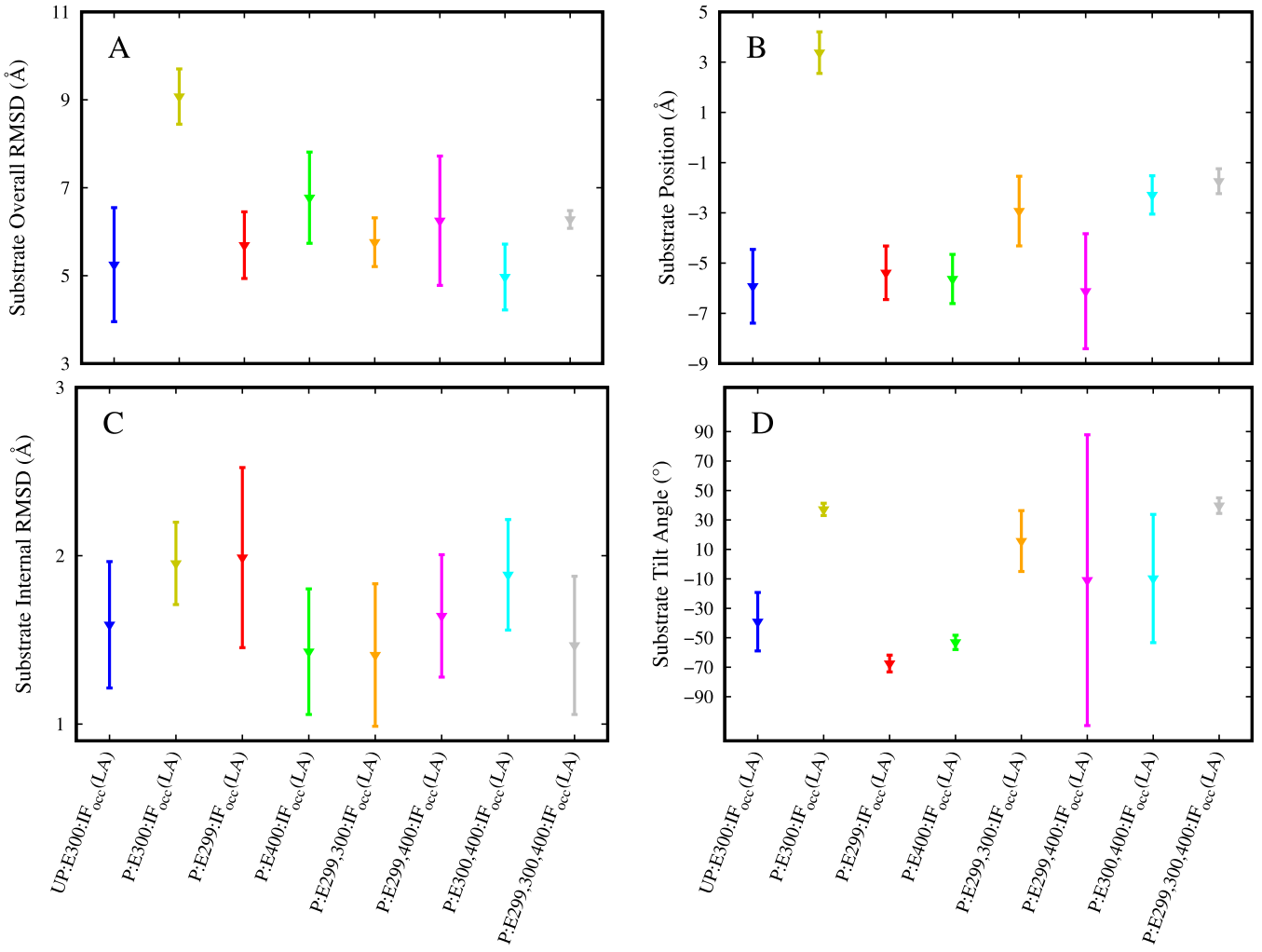

Figure 2. Effect of deprotonation/protonation of residues on the substrate overall (A) and internal (C) RMSDs, substrate position (B) along the membrane normal, and substrate tilt angle (D). In the P:E300:IF$_{occ}$(LA) system, the substrate moved up in the binding site, which is not seen in other systems (B). The "overall RMSD" of the substrate in the P:E300:IF$_{occ}$(LA) system was relatively higher compared to the other seven systems, which indicates that E300 is the most sensitive and important residue that plays a key role in PepT$_{St}$ dynamics (A). The last 800 ns of simulation data was included in this calculation.

bridge with R33 (that belongs to TM1) and stabilizing the IF conformation, at least in GkPOT and PepT$_{St}$.[1,17,19] It was also identified that R33 (or its equivalent) is important for proton-coupled transport in the GkPOT and PepT$_{St}$.[19] The R33−E300 salt bridge forms upon deprotonation of E300, bringing the two domains closer, and breaks when the E300 is protonated thus separating the two domains.[1,19] Therefore, protonation of E300 and subsequent breaking of the R33−E300 salt bridge are required for the protein transitioning from an IF/IF$_{occ}$ state to an OF state, which facilitates substrate entry. To test this hypothesis, we measured the R33−E300 salt bridge distance.

Our simulation data suggest that the R33−E300 salt bridge forms in PepT$_{St}$ upon deprotonation of the E300 as expected (Figures 1E and S1). In both the E300 deprotonated apo systems [i.e., UP:E300:OCC(Apo) and UP:E300:IF(Apo)], the R33−E300 salt bridge stabilized around 3 Å (Figures 1E and S1B,C). However, this salt bridge broke in the two apo E300 protonated systems [i.e., P:E300:OCC(Apo) and P:E300:IF(Apo)], and the distance fluctuated around 5−7 Å (Figures 1E and S1E,F). In the other four E300 protonated systems with the bound LA substrate [i.e., P:E300:IF$_{occ}$(LA), P:E299,300:IF$_{occ}$(LA), P:E300,400:IF$_{occ}$(LA), and P:E299,300,400:IF$_{occ}$(LA)], the R33−E300 salt bridge was broken as expected and the distances varied between 7 and 11 Å (Figures 1E and S1D,I,K,L). Particularly, in the P:E300:IF$_{occ}$(LA) system, it went up to 11 Å (Figures 1E and S1D); the LA substrate was situated between the two domains and interacting with R33 and E299 [as shown in the contact analysis (Table S1)]. This [P:E300:IF$_{occ}$(LA)] probably represents the OF state of the PepT$_{St}$ [Figures S2A and S6 (right panel)]. Also, this is probably the first step for the entry of the substrate into the substrate translocation site. In the two E300 protonated apo systems [i.e., P:E300:OCC(Apo) and P:E300:IF(Apo)], although the R33−E300 salt bridge was broken, R33 was engaging in salt bridge formation with E299 preventing the transition of the protein completely from an IF/IF$_{occ}$ state to an OF state (Figures 1F and S3E,F). Of note, the R33−E299 salt bridge was absent in the remaining ten systems (Figure 1E). Hence, we propose that for this protein to completely transition from an IF(apo) side to OF(apo) side, both E299 and E300 have to be protonated. Also, we propose that the two salt bridges (i.e., R33−E300 and R33−E299) act as a conformational switch for PepT$_{St}$ to transition from an

https://doi.org/10.1021/acs.jpcb.1c03982
J. Phys. Chem. B 2021, 125, 9738−9750

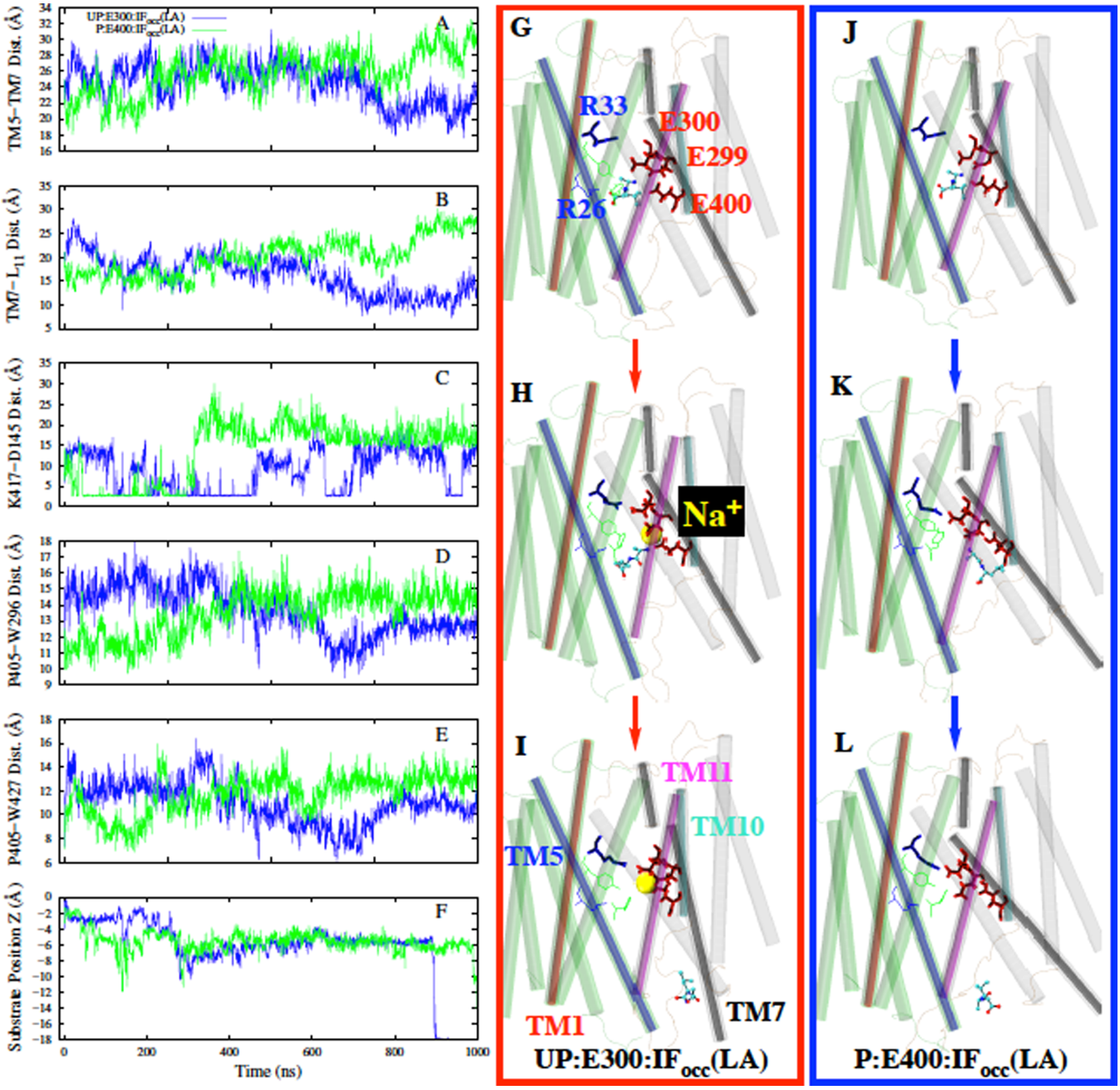

Figure 3. Pathway of substrate release. Shown in the left panels are various variables measured across the substrate transport path (A−F). Middle (G−I) and right panels (J−L) show the transportation of the LA substrate in the UP:E300:IF_{occ}(LA) and P:E400:IF_{occ}(LA) systems, respectively. All the variables are shown in Figure 1 in detail.

IF(Apo) state to an OF(Apo) state. In the four other holo systems with E300 deprotonated [i.e., UP:E300:IF_{occ}(LA), P:E299:IF_{occ}(LA), P:E400:IF_{occ}(LA), and P:E299,400:I-F_{occ}(LA)], the R33−E300 salt bridge was intact, although fluctuating often (Figures 1E and S1A,G,H,J). This forced the LA substrate toward the cytoplasmic side. Therefore, in the process of attaining a new optimal orientation/conformation, the LA substrate destabilizes the protein, particularly the R33−E300 salt bridge, because it often interacts with E300 and destabilizes the R33−E300 salt bridge (Table S1). When E299 or E400 was deprotonated, the LA substrate moved down toward the cytoplasmic side and interacted with these two residues; therefore, it is less likely that the LA substrate disturbs the R33−E300 salt bridge in these two systems. This was reflected in the P:E299:IF_{occ}(LA) and the P:E400:I-F_{occ}(LA) systems; in the first case, LA was interacting with the E400 (≈99% contact frequency), and in the second case, it was interacting with the E299 (≈91% contact frequency) (Table S1). In either case, E300 was not among the top 10 interacting residues with LA (Table S1). When E299 and/or E400 were not available, either due to protonation or other reasons, LA was engaging with the E300. This was reflected in the P:E299,400:IF_{occ}(LA) and UP:E300:IF_{occ}(LA) systems. In either case, LA was interacting with the E300 for at least 35% of the simulated time (Table S1). Overall, the four E300 deprotonated holo systems demonstrated that the LA substrate was not comfortable in the binding site when protein was in the IF_{occ} state; hence, it facilitates transitioning of the protein

https://doi.org/10.1021/acs.jpcb.1c03982
J. Phys. Chem. B 2021, 125, 9738−9750

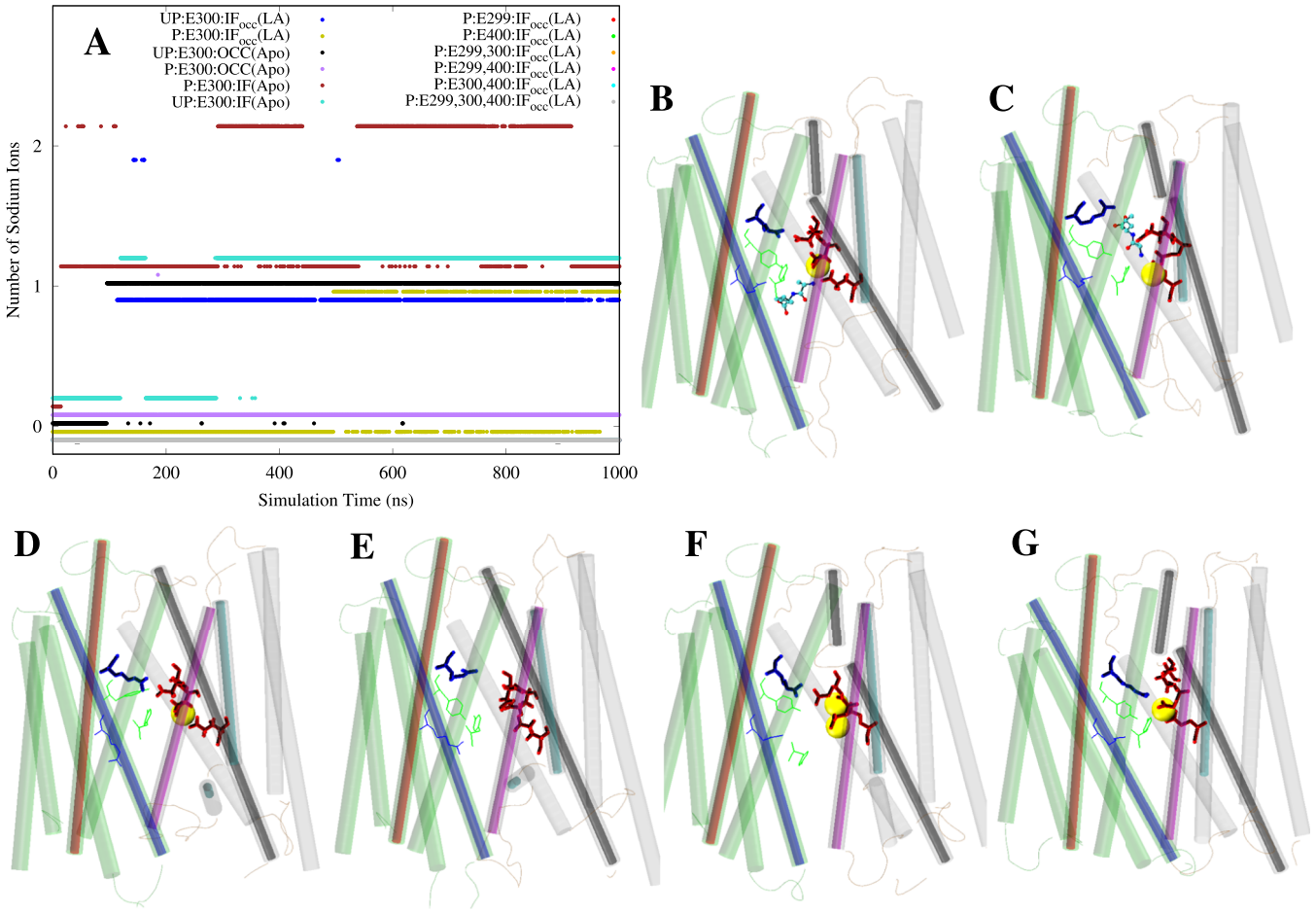

Figure 4. Sodium coordination of E299 and E400. Sodium ions within 4 Å of both E299 and E400 are shown. (A) Time series of sodium coordination. (B) UP:E300:IF$_{occ}$(LA), (C) P:E300:IF$_{occ}$(LA), (D) UP:E300:OCC(Apo), (E) P:E300:OCC(Apo), (F) UP:E300:IF(Apo), and (G) P:E300:IF(Apo). The sodium ions are represented as yellow spheres. Sodium coordination was not seen in the case of P:E300:OCC(Apo) (E).

completely toward the cytoplasmic side, which in turn facilitates the substrate transport. Here, comfortable binding refers to ligand stability within the binding site, which is discussed below in terms of substrate "overall root-mean-square deviation" (RMSD) and substrate-protein contact frequency analysis as well as the stability of the protein interdomain salt bridges that lock the transporter in a conformation that restricts the movement of the substrate in the binding site.

Deprotonation of E300 is Required for the Substrate to Get Transported toward the Cytoplasmic Side. As described earlier, of the eight holo systems, in half of them, E300 was deprotonated [i.e., UP:E300:IF$_{occ}$(LA), P:E299:IF$_{occ}$(LA), P:E400:IF$_{occ}$(LA), and P:E299,400:IF$_{occ}$(LA)]. We defined a variable Z to describe the position of the substrate along the membrane normal. $Z = 0$ represents the center of the membrane, and negative and positive values of Z represent the substrate on cytoplasmic and periplasmic sides, respectively. In these four systems, the substrate moved toward the cytoplasmic side (Figure 2B) because the N- and C-domains in the OF side are locked by the R33−E300 salt bridge. However, in the four E300 protonated holo systems [i.e., P:E300:IF$_{occ}$(LA), P:E299,300:IF$_{occ}$(LA), P:E300,400:IF$_{occ}$(LA), and P:E299,300,400:IF$_{occ}$(LA)], the substrate stayed more toward the OF side compared to the E300 deprotonated systems. The difference in the Z values of the substrate between the E300 deprotonated/protonated systems is such that their mean values are separated by more than their standard deviations (Figure 2B); the average Z values of all the E300 deprotonated systems sampled are around −6, and the Z values of E300 protonated systems are all above −3. This is because the R33−E300 salt bridge was broken in these systems (Figure 1E) providing more room for the substrate to move up the binding site and attain an ideal orientation. This was also reflected in the "overall RMSD" of the substrate (Figure 2A). The substrate "overall RMSD" is the relative change in the substrate RMSD with respect to its starting conformation, and this was calculated by aligning the protein against its starting conformation.[1] Although there was a sharp increase of the "overall RMSD" in the four holo E300 protonated systems in the beginning (Figure S4D,I,K,L), later they all stabilized compared to the four holo E300 deprotonated systems (Figure S4A,G,H,J). On the other hand, the "internal RMSD" depicts the conformational changes happening in the substrate and was measured by aligning the substrate against its own initial orientation. Internal RMSDs of substrates were fairly stable in all eight holo systems studied [fluctuated around 2.0 Å (Figures 2C and S4)], suggesting that there were no significant conformational changes in the substrate.

Among the four E300 deprotonated holo systems, the substrate was completely transported in two systems [i.e., in UP:E300:IF$_{occ}$(LA) and P:E400:IF$_{occ}$(LA)] toward the IF side,

https://doi.org/10.1021/acs.jpcb.1c03982
J. Phys. Chem. B 2021, 125, 9738−9750

as reflected by the sudden drop in the Z values of the substrate (Figure 3F), and in the other two holo systems [i.e., P:E299:IF$_{occ}$(LA) and P:E299,400:IF$_{occ}$(LA)], the substrate was translocated toward the IF side waiting to get transported (Z = ≈−6, Figure 2B). In the UP:E300:IF$_{occ}$(LA) and P:E400:IF$_{occ}$(LA) systems, the substrate attained a vertical orientation (Figure 3I,L) and then left the protein toward the IF side around 900 and 990 ns, respectively (Figure 3F), confirming that these were not favorable conditions for the binding of the LA substrate in the binding site and thus eventually got transported.

To assess the orientation of the LA substrate, we measured the tilt angle, which describes the deviation of the substrate from the membrane normal. Tilt angle zero indicates that the substrate attained a horizontal orientation, whereas negative or positive tilt angles indicate that the substrate attained a vertical orientation. Also, a negative tilt angle indicates that the C- and N-terminus face the cytoplasm and periplasm, respectively, and a positive tilt angle indicates the opposite. We have observed a correlation between the substrate tilt angle and protonation of E300. When E300 was protonated, the tilt angle was positive (i.e., C-terminus was facing the periplasmic side) and vice versa (i.e., C-terminus was facing the cytoplasmic side) (Figure 2D). The P:E299,400:IF$_{occ}$(LA) and P:E300,400:IF$_{occ}$(LA) systems were exceptions, where they undergo a range of fluctuations, as reflected by the large standard deviations.

Overall, we show that for the substrate to bind comfortably in the pocket, E300 has to be protonated. However, for the substrate to get transported, the formation of the R33−E300 salt bridge is mandatory, which in turn requires deprotonation of E300. When the R33−E300 salt bridge forms, it pushes the substrate toward the cytoplasmic side, leaving less room for the substrate to adjust to the binding site. Also, the R33−E300 salt bridge formation opens the protein toward the IF side (discussed in detail in the next section), exposing the substrate to water and eventually resulting in substrate transport toward the cytoplasmic side.

Disengaging E299 and E400 from Interacting with the Substrate is the Key for Releasing the Substrate toward the IF Side. We have observed that E299 and E400 play a key role in the transport of the LA substrate. These two residues act as the primary interaction sites for the substrate (Table S1) after it has been pushed down following deprotonation of E300 and the subsequent formation of the R33−E300 salt bridge, hence preventing the transport of substrate toward the cytoplasmic side at least temporarily. We identified two events that could circumvent this problem by disrupting the interaction of the residues E299 and E400 with the LA substrate and thus promote its transport: (1) coordination of the residues E299 and E400 by sodium ions and (2) protonation of E299 or E400 or both. Both events are discussed in detail below.

Sodium Modulation of Substrate Binding and Transport. Ions such as sodium,[30] calcium,[49,50] magnesium,[31,51] and zinc[51] play a key role in the body by modulating several therapeutically important receptors/proteins. Particularly, several membrane transporters rely on ions for transporting the substrate across the membrane bilayer, for example, the sodium-coupled transporters.[30] In this study, we observed sodium ions playing a role in the LA substrate transport. In 5 out of the 12 simulated systems, we have observed at least 1 sodium ion co-coordinating the E299 and E400 residues; two were holo systems [i.e., UP:E300:IF$_{occ}$(LA) and P:E300:IF$_{occ}$(LA)] and the remaining three were apo systems [i.e., UP:E300:OCC(Apo), UP:E300:IF(Apo), and P:E300:IF(Apo)] (Figure 4A). On a side note, for the sodium coordination to happen, both the residues E299 and E400 have to be deprotonated, which is the case with the five systems mentioned previously.

In the UP:E300:IF$_{occ}$(LA) system, E299 and E400 were coordinated by sodium, preventing them from engaging with the LA substrate (Table S1), thus facilitating the substrate transport. Additionally, in the UP:E300:IF$_{occ}$(LA) system, E300 was deprotonated; therefore, the R33−E300 salt bridge was intact, which pushed the substrate down and contributed to substrate transport. In the other substrate-bound system [i.e., the P:E300:IF$_{occ}$(LA)], although E299 and E400 were deprotonated and coordinated by sodium, the substrate was not transported. This may be because in this system, E300 was protonated; therefore, the R33−E300 salt bridge was not intact (Figure 1E), providing more room for the substrate to bind comfortably in the binding site between the residues R33 and E299. Hence, we propose that deprotonation of E300 alone is not enough for the transportation of the substrate and that the residues E299 and/or E400 should also be disengaged from the substrate. One way of achieving this is through sodium coordination of the residues E299 and E400, which is only possible when E299 and E400 are deprotonated as discussed earlier. In the seven other systems in which sodium coordination of E299 and E400 was not observed, either E299 or E400 or both were protonated hindering the coordination by sodium.

We note that sodium is not a known substrate of this transporter. We also note that sodium is not transported in our simulations, and so it is not considered a cotransported species. The key aspect of our proposed mechanism for the substrate transport toward the cytoplasm is that the residues E299 and E400 should disengage from interacting with the substrate, thereby facilitating the substrate release. We observed that this occurs in our simulations through either (1) protonation or (2) sodium coordination of residues E299 and E400. Whether the sodium coordination is relevant physiologically or not, we argue that the disengagement of these residues from the substrate is necessary for the substrate transport.

Protonation of E299/E400 Promoting Transport. We have demonstrated thus far that for the substrate to get transported toward the IF side, the R33−E300 salt bridge has to be intact, which is only possible when E300 is deprotonated. Our simulated set contains four E300 deprotonated holo systems, and in three of them, either E299 and/or E400 were protonated [i.e., P:E299:IF$_{occ}$(LA), P:E400:IF$_{occ}$(LA), and P:E299,400:IF$_{occ}$(LA)]. We previously showed that in the UP:E300:IF$_{occ}$(LA) system, the substrate got transported toward the IF side. Also, in the P:E400:IF$_{occ}$(LA) system, the substrate completely left the pocket (Figure 3F). In the remaining two systems [i.e., in P:E299:IF$_{occ}$(LA) and P:E299,400:IF$_{occ}$(LA)], the substrate moved down the binding site and was about to leave as reflected by the Z values of the substrate (Figure 2B). In the P:E299:IF$_{occ}$(LA) system, although E299 was protonated, the substrate did not leave in a 1 μs simulation because E400 was interacting with the substrate and preventing it from leaving as shown in contact frequency analysis (99% interaction frequency, Table S1). Lastly, in the P:E299,400:IF$_{occ}$(LA) system, the substrate was engaging with the residues R26, Y68, and E300 (Table S1), and hence, it was not transported. This was also reflected in

https://doi.org/10.1021/acs.jpcb.1c03982
J. Phys. Chem. B 2021, 125, 9738−9750

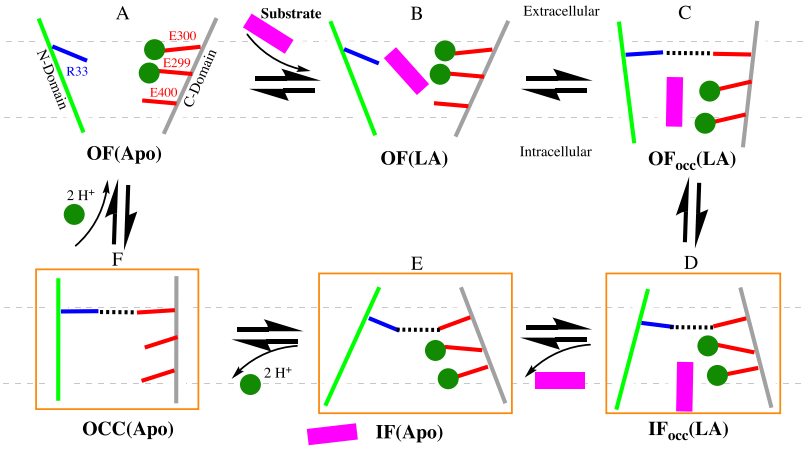

Figure 5. Proposed transport cycle. X-ray crystal conformations that are simulated in this study are inserted in orange boxes (D−F). N- and C-domains are colored in green and gray, respectively. R33 is colored blue, and E299, E300, and E400 are colored red. The LA substrate is colored in magenta, and the protons are shown as green spheres. The membrane bilayer is shown as broken gray lines. Substrate binds when the protein is in the OF conformation (B). Formation of the R33−E300 salt bridge pushes the substrate toward the IF side (C). This is only possible when the proton that is attached to E300 is displaced. Formation of this R33−E300 salt bridge forces the protein to attain an IF$_{occ}$(LA) conformation (D). Protonation of the residues E299/E400 and deprotonation of E300 favor the substrate to be released into the IF side (D), resulting in an IF(Apo) conformation (E). Ideally, protonation of both E299 and E400 is better for the substrate release; however, protonation of either one of them is sufficient. We have observed substrate release in the system with E300/E299 deprotonated and E400 protonated [P:E400:IF$_{occ}$(LA)]. Another situation for the substrate release that we have observed was when E299/E300/E400 was deprotonated [UP:E300:IF$_{occ}$(LA)]. This is similar to panel (D), except that E299 and E400 are deprotonated. In the UP:E300:IF$_{occ}$(LA) system, we have observed sodium coordinating the residues E299 and E400, preventing them from interacting with the substrate, which in turn facilitated the substrate release (not shown in this cycle for clarity purpose). The release of the substrate, followed by the protons facilitates the protein to attain an OCC(Apo) state (F). The binding of protons to E299 and E300 of the OCC(Apo) state facilitates the protein to transition to an OF(Apo) state (A). Protonation of these two residues disrupts the R33−E299 and R33−E300 salt bridges, hence facilitating the conformational transition. Therefore, we propose that these two salt bridges act as a "conformational switch" for this OCC(Apo) to OF(Apo) transition.

the R33−E300 salt bridge distance; the LA substrate disrupted this salt bridge (Figure S1J) while interacting with the residue E300 (Table S1). We demonstrated here that deprotonation of E300 and protonation of E299/E400 facilitate transport because the protonated E299/E400 disengage themselves from the substrate.

Favorable Conditions for Substrate Transport. Based on the observations made in this study (as discussed above), systems that are ideal for the substrate to get transported are (1) UP:E300:IF$_{occ}$(LA), (2) P:E400:IF$_{occ}$(LA), (3) P:E299:IF$_{occ}$(LA), and (4) P:E299,400:IF$_{occ}$(LA). The common factor among these four systems is that E300 is deprotonated; hence, the R33−E300 salt bridge is intact (Figures 1E,F and S1) in all these systems. Therefore, the substrate was pushed down the translocation path waiting to get transported (Figure 2B), which establishes that the R33−E300 salt bridge formation is important for the substrate release. In the first case [i.e., the UP:E300:IF$_{occ}$(LA)], the coordination of E299/E400 with a sodium ion (Figure 4A) prevents the substrate from interacting with the residues E299 and E400 (Table S1), thus facilitating the substrate release. In case 2 [i.e., the P:E400:IF$_{occ}$(LA)], because E400 was protonated, it was not interacting with the substrate. Although E299 was deprotonated and engaging with the substrate blocking its release (Table S1, 90% contact frequency), stacking of E299 between the residues E300 and E400 was preventing it from holding the substrate for long, thus facilitating its release. In case 3 [i.e., the P:E299:IF$_{occ}$(LA)], the substrate moved down the pocket and was waiting to get released (Figure 2B). In this system, E400 (which is deprotonated) engages with the substrate (Table S1, 98% contact frequency) impeding its release, whereas the E299 cannot engage with the substrate because it was protonated. In case 4 [i.e., the P:E299,400:IF$_{occ}$(LA)], both E299 and E400 were protonated and, hence, cannot engage with the substrate. Instead, the substrate was interacting with the residues R26, Y68, and E300 with 42, 71, and 38% contact frequencies, respectively (Table S1). The substrate moved toward the IF side (Figure 2B) and was not stable as reflected by the "overall RMSD" (Figure S4J) and was waiting to get transported toward the IF side. Overall, we show that the ideal scenario for the substrate to get transported is through the deprotonation of E300 and disengaging E299 and/or E400 from interacting with the substrate (either through sodium coordination or protonation).

A hypothetical transport cycle based on these findings is shown schematically in Figure 5. In brief, all three titratable residues (i.e., E299, E300, and E400) that are lining the substrate-binding site are important for binding and transport. We propose that the optimum condition for the substrate to get transported toward the cytoplasmic side after binding in the substrate-binding site is when E300 is deprotonated and E299 and E400 are protonated. E300 deprotonation keeps the R33−E300 salt bridge intact pushing the substrate toward the cytoplasmic side. If the residues E299 and/or E400 are deprotonated, the substrate can interact with these residues blocking its transport. Therefore, if these two residues (E299 and E400) are protonated, the substrate cannot engage with them and thus gets transported toward the IF side. In the two systems in which the substrate got transported [UP:E300:IF$_{occ}$(LA) and P:E400:IF$_{occ}$(LA)], E300 is deprotonated. The key to our proposed mechanism is E300 being deprotonated and that the residues E299/E400 disengage with the substrate. We have observed in our study that disengaging E299 and E400 from interacting with the substrate happened when (1)

https://doi.org/10.1021/acs.jpcb.1c03982
J. Phys. Chem. B 2021, 125, 9738−9750

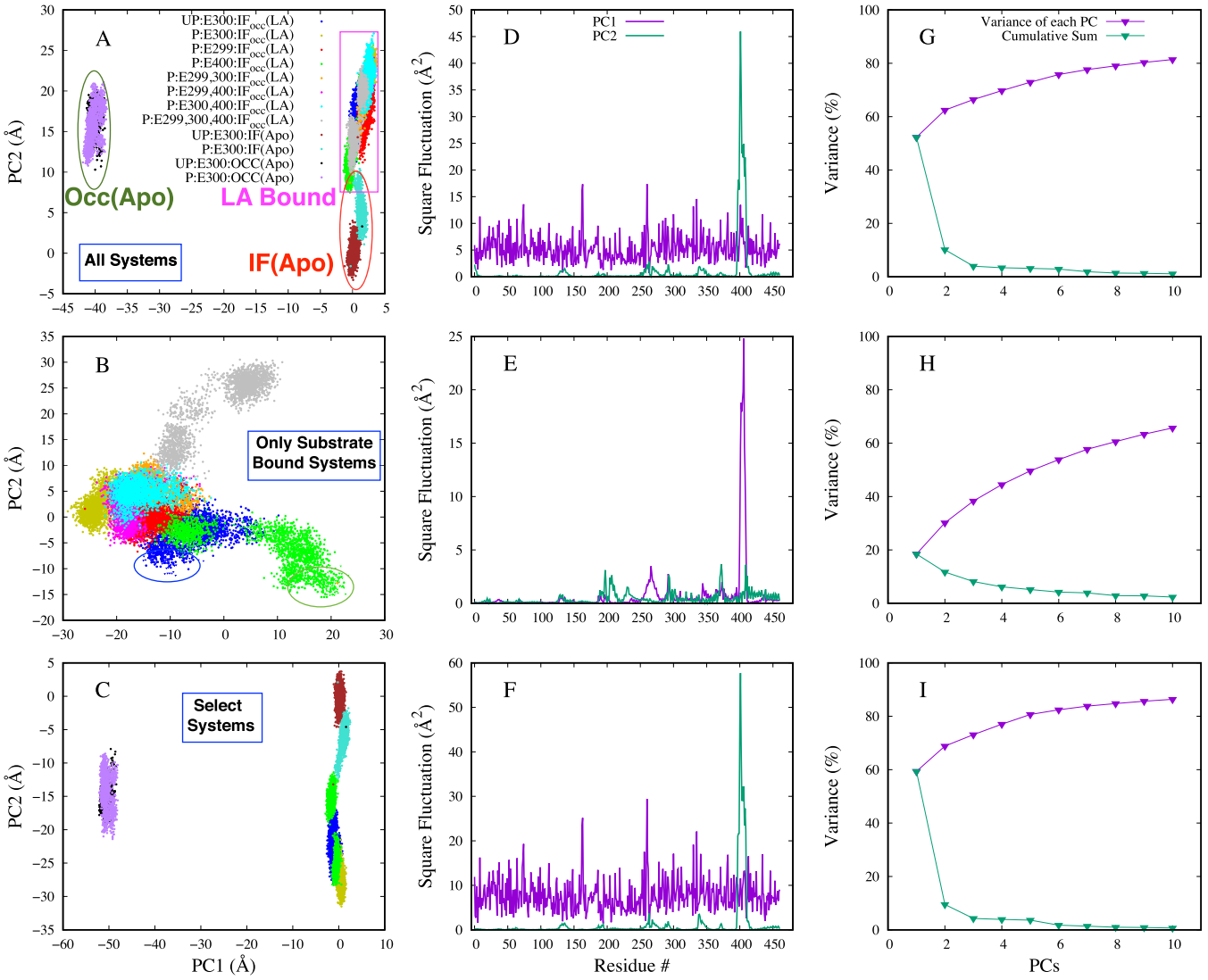

Figure 6. PCA. Left panels are the projection of data onto the PC1 and PC2 space. Each panel is based on independent PCA analysis using the entire 1 μs trajectories of all systems (A), or only the substrate-bound systems (B), or a select number of systems of interest (C). In each case, all trajectories used to build the PCs were projected. UP:E300:IF(Apo) was used as a reference structure for PCA in panels (A) and (C), whereas UP:E300:IF$_{occ}$(LA) was used as a reference structure for PCA in panel (B). Data points highlighted in circles (B) represent the protein conformations when the substrate leaves the protein and moves into the cytoplasmic side. Middle panels (D–F) are square displacements of PC1 (purple) and PC2 (green) modes as a function of the residue number. Right panels (G–I) depict the proportion of variance of the top 10 modes in each case (green). The purple-colored data points represent the cumulative average of the top 10 PC modes. Only C_α atoms were considered for these calculations.

one of these two residues were protonated or (2) when these two residues were interacting with the sodium ion.

Impact of Deprotonation/Protonation on Protein Conformational Dynamics is Captured in PCA. We monitored the impact of deprotonation/protonation at the global level (i.e., on the entire protein). To assess the stability and also to identify major conformational changes, we measured the backbone RMSD of the protein. In all 12 cases, the protein reached equilibrium, and RMSDs of all systems stabilized around 3 Å (Figure S4). Protein RMSDs did not provide any evidence of large conformational changes at the global level.

Further, to assess the conformational landscape of the 12 systems, we employed PCA analysis.[31,52] The impact of protonation/deprotonation on the protein conformation was clearly observed in the PCA analysis. When all 12 structures were projected onto a PC space built based on all trajectories, PC1 clearly differentiated the systems into two distinguished clusters (Figure 6A). Cluster-1 includes the two occluded-(Apo) structures, and cluster-2 consists of the rest of the ten remaining systems [i.e., the IF(Apo) and the IF$_{occ}$ (LA bound)]. The trajectories were clustered into three groups in the PC2 space; one cluster formed by the P:E300:IF(Apo), the second by the UP:E300:IF(Apo), and the third by the rest. Square displacements have been calculated to identify the major contributions to the individual PC components. PC1 for the entire 12 system trajectory had contributions almost from all domains indicating a truly global conformational variability. Specific residues with higher contributions included residues 163–164 (TM5) and 261 (that belongs to a helix outside the N- and C-domains) (Figure 6D), whereas PC2 was dominated by the residues 400–410 (loop between helices TM10 and TM11). PC1 and PC2 contribute ≈52 and ≈10% (Figure 6G) to the total variance, respectively. When only substrate-bound

https://doi.org/10.1021/acs.jpcb.1c03982
J. Phys. Chem. B 2021, 125, 9738–9750

systems were used to perform PCA, four clusters were observed; P:E400:IF_{occ}(LA) was in the first cluster, UP:-E300:IF_{occ}(LA) in the second, P:E299,300,400:IF_{occ}(LA) in the third, and the fourth cluster comprised the rest (Figure 6B). PC1 clearly differentiates P:E400:IF_{occ}(LA) and UP:-E300:IF_{occ}(LA) structures when the substrates are released (Figure 6B, shown in blue and green circles), indicating that these systems adopt different conformations when they release the substrates. Square displacements of just holo trajectories were dominated by the C-domain in both the PC1 and PC2 modes (Figure 6E). However, the first two PCs contribute only ≈30% to the total variation, which indicates that variation for this PC space was multifold (Figure 6H). When OCC(Apo), IF(Apo), UP:E300:IF_{occ}(LA), P:E300:IF_{occ}(LA), and P:E400:IF_{occ}(LA) were combined to perform another independent PCA, both UP:E300:IF_{occ}(LA) and P:E400:I-F_{occ}(LA) were clustered differently from the IF(Apo) systems on the PC2 space. This indicates that the UP:E300:IF_{occ}(LA) and P:E400:IF_{occ}(LA) structures were not as open as the IF(Apo) systems when the substrate was released (Figure 6C). An interesting common feature in all the three PC spaces built based on different trajectories (i.e., top, middle, and bottom panels) is that a common region of the protein (i.e., the TM10−TM11 loop region) has a significant contribution to the variability either in PC1 or PC2. This observation indicates the importance of TM10 and TM11, as will be discussed in more detail below. Overall, PCA analysis highlights the sensitivity of POT structure and conformational dynamics upon protonation/deprotonation of a select few important residues. More importantly, this analysis also highlights that POTs can adopt different conformations while they release the substrate depending on the situation, which is also a known feature of the POT family of transporters.[18]

Additionally, we calculated different variables to quantify global dynamics of the protein such as the N-,C- interdomain angle (Figure 1D), TM1−TM7 and TM5−TM11 interhelical angles (Figure 1A), and $L_{4,5}$−$L_{10,11}$ distance (Figure 1B).[1] $L_{4,5}$ is a loop between the helices 4 and 5, and $L_{10,11}$ is a loop between the helices 10 and 11 on the cytoplasmic side. The $L_{4,5}$−$L_{10,11}$ distance quantifies the opening of the protein on the cytoplasmic side.[1] According to this measure, the major impact of protonation was observed in the case of the IF(Apo) systems (Figure S2D); the opening of the protein on the cytoplasmic side was greater in the UP:E300:IF(Apo) system compared to the P:E300:IF(Apo) system, and their estimated mean distances were separated by more than their standard deviations. Similar behavior was observed in the Occ(Apo) systems. Overall, in the apo systems (IF or OCC), E300 deprotonation makes the protein open more toward the cytoplasm than E300 protonation. However, this trend was reversed in the holo systems, except in the case of P:E299:IF_{occ}(LA). This behavior hints that the substrate binding favors more of an occluded conformation when E300 is protonated. The difference between different substrate-bound systems is not significant. The N-,C- interdomain angle indicates the opening between the two domains on the cytoplasmic side (Figure 1D). The behavior of this variable was similar to the $L_{4,5}$−$L_{10,11}$ distance in the case of IF(apo) systems. The difference in the N-,C- interdomain angle between the UP:E300:IF(Apo) and P:E300:IF(Apo) systems was ≈7°, and in the remaining 10 systems, no conclusive trend was observed (Figure S2A). Similar behavior was observed in the case of TM1−TM7 (Figure S2B) and TM5−TM11 (Figure S2C) interhelical angles as well. The TM1−TM7 interhelical angle is a hypothesized cytoplasmic gate, whereas the TM5-TM11 interhelical angle is a hypothesized periplasmic gate (Figure 1A).

Helices 5, 7, 10, and 11 Play a Key Role in the Substrate Transport toward the IF Side. Based on the two substrate release simulations [i.e., UP:E300:IF_{occ}(LA) and P:E400:IF_{occ}(LA)], we mapped the substrate transport pathway in $PepT_{St}$. We propose that this transition occurs in three stages.

In stage one, the substrate undergoes an orientation change, that is, from horizontal to vertical (Figure 3H,K). In the vertical orientation, the C-terminus and the N-terminus of the substrate were facing the cytoplasmic and the periplasmic sides, respectively [which was also shown through the tilt angle (Figure 2D)], because the substrate prefers to interact with the negatively charged residues (i.e., E299, E300, and E400) on the periplasmic side via the N-terminus. This behavior is very similar to the GkPOT.[1] Note that the substrate is in a horizontal orientation in the crystal structures (Figure 3G,J).

In stage two, the opening of the hydrophobic bridge facilitates a downward movement of the substrate along the translocation path. This hydrophobic bridge is formed by the residues W296 (TM7), P405 (TM10), and W427 (TM11). These three residues belong to the C-domain and are located in the middle of the protein right below the substrate-binding site (Figure 1C) and prevent the release of the substrate toward the IF side. Earlier it was reported that mutation of W427 to alanine drastically reduced the proton/peptide drive counter flow uptake.[17] To map the opening and closing of this hydrophobic bridge, we measured two different distances between (1) the residues P405 and W427 and (2) the residues P405 and W296 (Figure 1C). Both these distances increased (Figure 3 D,E) at the time of the substrate transport (i.e., at the end of the simulation) toward the intracellular side, which establishes that the opening of this hydrophobic gate is crucial for the transport of the substrate. However, the extent of the opening is greater in the case of P:E400:IF_{occ}(LA) than in the P:E400:IF_{occ}(LA).

In stage three, helices 5, 7, and 11 moved away from each other at the cytoplasmic side facilitating the release of the substrate. To quantify this behavior, we measured the distance between the tips of TM5 (considered residues 144 and 145) and TM7 (considered residues 280 and 281). Additionally, we measured the distance between the tips of TM7 (considered residues 280, 281) and TM11 (considered residues 418, 419 that are part of the loop) (Figure 1C). In the P:E400:IF_{occ}(LA) simulation both these distances consistently increased with time (Figure 3A,B). In the case of the UP:E300:IF_{occ}(LA) system, unlike in the P:E400:IF_{occ}(LA), there was a drastic increase in both of these values during the first 100 ns and then gradually decreased with time and slightly increased while the substrate was released into the cytoplasmic side (i.e., around 900 ns). However, the final values of these two measures for this system were greater than the initial values (i.e., in the crystal structure). Overall, the opening of the transporter was greater on the cytoplasmic side during the substrate release in P:E400:IF_{occ}(LA) than in UP:E300:IF_{occ}(LA). We also observed a salt bridge breaking on the cytoplasmic side [i.e., D145 (TM5)-K417 (TM11)] (Figure 1C) in both the systems facilitating the transport (Figure 3C).

Overall, our results indicate that the TM helices 5, 7, 10, and 11 play a key role in the transportation of the substrate toward

https://doi.org/10.1021/acs.jpcb.1c03982
J. Phys. Chem. B 2021, 125, 9738−9750

the cytoplasmic side after it binds in the substrate-binding site. Helices 7, 10, and 11 belong to the C-domain, and helix 5 belongs to the N-domain. Therefore, we conclude that the C-domain dominates the transportation process rather than the N-domain. This was also reflected in root-mean-square fluctuation (RMSF) calculations, which indicate that the C-domain fluctuates relatively more than the N-domain in all the holo systems (Figure S5B,C). Particularly in the P:E400:I-F_{occ}(LA) system, the region spanning residues 400−425 (loop between TM helices 10 and 11) fluctuates greater (≈7 Å) (Figure S5C) compared to all other systems indicating that this region plays a key role in the transport process in this system. This also means that there are more interaction sites for the substrate in the C-domain than in the N-domain. On a side note, in the IF(Apo) systems, the N-domain fluctuated more than the C-domain, whereas in the OCC(Apo) systems, fluctuations of both domains were comparable (Figure S5A). The OCC and IF forms majorly differ in the C-domain (spanning residues 400−425); this region fluctuates to a greater extent in the OCC than in the IF systems. The finding that the increase in flexibility of the C-domain relative to the N-domain was not observed in the IF structures is rather interesting as it may suggest that it was the interaction of the substrate with the C-domain that triggers the increased dynamics and not the other way around. This was in contrast to a report by Fowler et al., which was based on short MD simulations (total 1.2 μs) of IF(Apo) crystal structures[24] that in both $PepT_{So}$ and $PepT_{St}$ dynamics of the C-domain dominates the N-domain. Such substrate-induced flexibility could perhaps be mechanistically relevant. The asymmetric dynamics of the N- and C-domains observed in this study suggest that the $PepT_{St}$ might not fit into the rocker and switch model, which was proposed earlier to describe the functioning of the transporter.[3,16] It is possible that any single model may not completely explain the entire transport process in the POTs, particularly $PepT_{St}$. In a study focused on lactose permease (LacY), another member of the MFS family of transporters, Stelzl et al. argued against the rocker and switch mechanism.[53]

CONCLUSIONS

In this study, we investigated the chemomechanical coupling involved in the substrate/proton transport of the $PepT_{St}$ transporter via microsecond-level MD simulations. The key observations made in this study are that (a) deprotonation/protonation of E300 is a must for the protein to bind and transport the substrate, (b) disengaging residues E299 and E400 from interacting with the substrate promotes the release of the substrate toward the cytoplasmic side, and (c) the interaction of R33 with E299 and E300 acts as a molecular switch for the complete transition of the protein from the IF state to the OF state. Additionally, we identified that the C-domain plays a major role in the functioning of the transporter, particularly TMs 7, 10, and 11, probably due to more interaction sites for the substrate on the C-domain compared to the N-domain. Finally, we report that the protein in all the eight substrate-bound systems (that differ in deprotonation/protonation of residues E299, E300, and E400) have different conformations from the crystal structure, indicating that there exist more physiologically relevant protonation states of the transporter apart from the ones studied here.

ASSOCIATED CONTENT

Supporting Information

The Supporting Information is available free of charge at https://pubs.acs.org/doi/10.1021/acs.jpcb.1c03982.

Time series of the R33−E300 salt bridge distance; impact of deprotonation/protonation on protein; time series of the R33−E299 distance; substrate and protein contact frequency; RMSD time series; RMSF versus residue number; and substrate orientations in different protonation states (PDF)

AUTHOR INFORMATION

Corresponding Author

Mahmoud Moradi − *University of Arkansas, Fayetteville, Arkansas 72701, United States;* orcid.org/0000-0002-0601-402X; Email: moradi@uark.edu

Author

Kalyan Immadisetty − *Stritch School of Medicine, Maywood, Illinois 60153, United States;* orcid.org/0000-0001-8261-6770

Complete contact information is available at: https://pubs.acs.org/10.1021/acs.jpcb.1c03982

Notes

The authors declare no competing financial interest.

ACKNOWLEDGMENTS

This research was supported by National Science Foundation grant CHE 1945465 and the Arkansas Biosciences Institute. This research is part of the Blue Waters sustained-petascale computing project, which was supported by the National Science Foundation (awards OCI-0725070 and ACI-1238993) and the state of Illinois. This work also used the Extreme Science and Engineering Discovery Environment (allocation MCB150129), which is supported by National Science Foundation grant number ACI-1548562. This research was also supported by the Arkansas High Performance Computing Center, which is funded through multiple National Science Foundation grants and the Arkansas Economic Development Commission.

REFERENCES

(1) Immadisetty, K.; Hettige, J.; Moradi, M. What can and cannot be learned from molecular dynamics simulations of bacterial proton-coupled oligopeptide transporter GkPOT? *J. Phys. Chem. B* **2017**, *121*, 3644−3656.

(2) Ito, K.; Hikida, A.; Kawai, S.; Lan, V. T.; Motoyama, T.; Kitagawa, S.; Yoshikawa, Y.; Kato, R.; Kawarasaki, Y. Analysing the substrate multispecificity of a proton-coupled oligopeptide transporter using a dipeptide library. *Nat. Commun.* **2013**, *4*, 2502.

(3) Lyons, J. A.; Parker, J. L.; Solcan, N.; Brinth, A.; Li, D.; Shah, S. T.; Caffrey, M.; Newstead, S. Structural basis for polyspecificity in the POT family of proton-coupled oligopeptide transporters. *EMBO Rep.* **2014**, *15*, 886−893.

(4) Newstead, S. Recent advances in understanding proton coupled peptide transport via the POT family. *Curr. Opin. Struct. Biol.* **2017**, *45*, 17−24.

(5) Parker, J. L.; Mindell, J. A.; Newstead, S. Thermodynamic evidence for a dual transport mechanism in a POT peptide transporter. *Elife* **2014**, *3*, No. e04273.

(6) Prabhala, B. K.; Aduri, N. G.; Hald, H.; Mirza, O. Investigation of the substrate specificity of the proton coupled peptide transporter

PepT So from Shewanella oneidensis. *Int. J. Pept. Res. Ther.* **2015**, *21*, 1−6.
(7) Guettou, F.; Quistgaard, E. M.; Trésaugues, L.; Moberg, P.; Jegerschöld, C.; Zhu, L.; Jong, A. J. O.; Nordlund, P.; Löw, C. Structural insights into substrate recognition in proton-dependent oligopeptide transporters. *EMBO Rep.* **2013**, *14*, 804−810.
(8) Jensen, J. M.; Simonsen, F. C.; Mastali, A.; Hald, H.; Lillebro, I.; Diness, F.; Olsen, L.; Mirza, O. Biophysical characterization of the proton-coupled oligopeptide transporter YjdL. *Peptides* **2012**, *38*, 89−93.
(9) Newstead, S. Molecular Insights into Proton Coupled Peptide Transport in the PTR Family of Oligopeptide Transporters. *Biochim. Biophys. Acta, Gen. Subj.* **2015**, *1850*, 488−499.
(10) Smith, D. E.; Clémençon, B.; Hediger, M. A. Proton-coupled oligopeptide transporter family SLC15: Physiological, pharmacological and pathological implications. *Mol. Aspects Med.* **2013**, *34*, 323−336.
(11) Meredith, D.; Boyd, C. A. R. Structure and function of eukaryotic peptide transporters. *Cell. Mol. Life Sci.* **2000**, *57*, 754−778.
(12) Rautio, J.; Kumpulainen, H.; Heimbach, T.; Oliyai, R.; Oh, D.; Järvinen, T.; Savolainen, J. Prodrugs: design and clinical applications. *Nat. Rev. Drug Discovery* **2008**, *7*, 255−270.
(13) Brandsch, M. Drug transport via the intestinal peptide transporter PepT1. *Curr. Opin. Pharmacol.* **2013**, *13*, 881−887.
(14) Anderson, C. M. H.; Thwaites, D. T. Hijacking solute carriers for proton-coupled drug transport. *Physiology* **2010**, *25*, 364−377.
(15) Jung, D.; Dorr, A. Single-dose pharmacokinetics of valganciclovir in HIV-and CMV-seropositive subjects. *J. Clin. Pharmacol.* **1999**, *39*, 800−804.
(16) Newstead, S.; Drew, D.; Cameron, A. D.; Postis, V. L. G.; Xia, X.; Fowler, P. W.; Ingram, J. C.; Carpenter, E. P.; Sansom, M. S. P.; McPherson, M. J.; et al. Crystal structure of a prokaryotic homologue of the mammalian oligopeptide-proton symporters, PepT1 and PepT2. *EMBO J.* **2011**, *30*, 417−426.
(17) Solcan, N.; Kwok, J.; Fowler, P. W.; Cameron, A. D.; Drew, D.; Iwata, S.; Newstead, S. Alternating access mechanism in the POT family of oligopeptide transporters. *EMBO J.* **2012**, *31*, 3411−3421.
(18) Martinez Molledo, M.; Quistgaard, E. M.; Flayhan, A.; Pieprzyk, J.; Löw, C. Multispecific substrate recognition in a proton-dependent oligopeptide transporter. *Structure* **2018**, *26*, 467−476.
(19) Doki, S.; Kato, H. E.; Solcan, N.; Iwaki, M.; Koyama, M.; Hattori, M.; Iwase, N.; Tsukazaki, T.; Sugita, Y.; Kandori, H.; et al. Structural basis for dynamic mechanism of proton-coupled symport by the peptide transporter POT. *Proc. Natl. Acad. Sci.* **2013**, *110*, 11343−11348.
(20) Jardetzky, O. Simple allosteric model for membrane pumps. *Nature* **1966**, *211*, 969−970.
(21) Ural-Blimke, Y.; Flayhan, A.; Strauss, J.; Rantos, V.; Bartels, K.; Nielsen, R.; Pardon, E.; Steyaert, J.; Kosinski, J.; Quistgaard, E. M.; et al. Structure of prototypic peptide transporter DtpA from E. coli in complex with valganciclovir provides insights into drug binding of human PepT1. *J. Am. Chem. Soc.* **2019**, *141*, 2404−2412.
(22) Martinez Molledo, M.; Quistgaard, E. M.; Löw, C. Tripeptide binding in a proton-dependent oligopeptide transporter. *FEBS Lett.* **2018**, *592*, 3239−3247.
(23) Aduri, N. G.; Prabhala, B. K.; Ernst, H. A.; Jørgensen, F. S.; Olsen, L.; Mirza, O. Salt Bridge Swapping in the EXXERFXYY Motif of Proton-coupled Oligopeptide Transporters. *J. Biol. Chem.* **2015**, *290*, 29931−29940.
(24) Fowler, P. W.; Orwick-Rydmark, M.; Radestock, S.; Solcan, N.; Dijkman, P. M.; Lyons, J. A.; Kwok, J.; Caffrey, M.; Watts, A.; Forrest, L. R.; et al. Gating Topology of the Proton-Coupled Oligopeptide Symporters. *Structure* **2015**, *23*, 290−301.
(25) Radestock, S.; Forrest, L. R. The Alternating-Access Mechanism of MFS Transporters Arises from Inverted-Topology Repeats. *J. Mol. Biol.* **2011**, *407*, 698−715.
(26) Forrest, L. R. (Pseudo-)Symmetrical Transport. *Science* **2013**, *339*, 399−401.
(27) Quistgaard, E. M.; Molledo, M. M.; Löw, C. Structure determination of a major facilitator peptide transporter: inward facing PepTSt from Streptococcus thermophilus crystallized in space group P3121. *PLoS One* **2017**, *12*, No. e0173126.
(28) Parker, J. L.; Li, C.; Brinth, A.; Wang, Z.; Vogeley, L.; Solcan, N.; Ledderboge-Vucinic, G.; Swanson, J. M. J.; Caffrey, M.; Voth, G. A.; Newstead, S. Proton movement and coupling in the POT family of peptide transporters. *Proc. Natl. Acad. Sci.* **2017**, *114*, 13182−13187.
(29) Samsudin, F.; Parker, J. L.; Sansom, M. S. P.; Newstead, S.; Fowler, P. W. Accurate prediction of ligand affinities for a proton-dependent oligopeptide transporter. *Cell Chem. Biol.* **2016**, *23*, 299−309.
(30) Immadisetty, K.; Madura, J. A review of monoamine transporter-ligand interactions. *Curr. Comput.-Aided Drug Des.* **2013**, *9*, 556−568.
(31) Immadisetty, K.; Hettige, J.; Moradi, M. Lipid-Dependent Alternating Access Mechanism of a Bacterial Multidrug ABC Exporter. *ACS Central Science* **2019**, *5*, 43−56.
(32) Ogden, D.; Immadisetty, K.; Moradi, M. Conformational Transition Pathways in Major Facilitator Superfamily Transporters. **2019**, bioRxiv:10.1101/708289.
(33) Harkey, T.; Govind Kumar, V.; Hettige, J.; Tabari, S. H.; Immadisetty, K.; Moradi, M. The Role of a Crystallographically Unresolved Cytoplasmic Loop in Stabilizing the Bacterial Membrane Insertase YidC2. *Sci. Rep.* **2019**, *9*, 14451.
(34) Chemical Computing Group Inc. *Molecular Operating Environment (MOE)*, 2013. 08 2016.
(35) Lomize, M. A.; Pogozheva, I. D.; Joo, H.; Mosberg, H. I.; Lomize, A. L. OPM database and PPM web server: resources for positioning of proteins in membranes. *Nucleic Acids Res.* **2012**, *40*, D370−D376.
(36) Lee, J.; Cheng, X.; Swails, J. M.; Yeom, M. S.; Eastman, P. K.; Lemkul, J. A.; Wei, S.; Buckner, J.; Jeong, J. C.; Qi, Y.; et al. CHARMM-GUI Input Generator for NAMD, GROMACS, AMBER, OpenMM, and CHARMM/OpenMM Simulations using the CHARMM36 Additive Force Field. *J. Chem. Theory Comput.* **2016**, *12*, 405−413.
(37) Jorgensen, W. L.; Chandrasekhar, J.; Madura, J. D.; Impey, R. W.; Klein, M. L. Comparison of simple potential functions for simulating liquid water. *J. Chem. Phys.* **1983**, *79*, 926−935.
(38) Reid, J. K. In *Large Sparse Sets of Linear Equations*; Reid, J. K., Ed.; Academic Press: London, 1971; pp 231−254.
(39) Jo, S.; Kim, T.; Im, W. Automated builder and database of protein/membrane complexes for molecular dynamics simulations. *PLoS One* **2007**, *2*, No. e880.
(40) Phillips, J. C.; Braun, R.; Wang, W.; Gumbart, J.; Tajkhorshid, E.; Villa, E.; Chipot, C.; Skeel, R. D.; Kalé, L.; Schulten, K. Scalable Molecular Dynamics with NAMD. *J. Comput. Chem.* **2005**, *26*, 1781−1802.
(41) Humphrey, W.; Dalke, A.; Schulten, K. VMD—Visual Molecular Dynamics. *J. Mol. Graphics* **1996**, *14*, 33−38.
(42) Klauda, J. B.; Venable, R. M.; Freites, J. A.; O'Connor, J. W.; Tobias, D. J.; Mondragon-Ramirez, C.; Vorobyov, I.; MacKerell, A. D., Jr.; Pastor, R. W. Update of the CHARMM all-atom additive force field for lipids: validation on six lipid types. *J. Phys. Chem. B* **2010**, *114*, 7830−7843.
(43) Martyna, G. J.; Tobias, D. J.; Klein, M. L. Constant pressure molecular dynamics algorithms. *J. Chem. Phys.* **1994**, *101*, 4177−4189.
(44) Feller, S. E.; Zhang, Y.; Pastor, R. W.; Brooks, B. R. Constant pressure molecular dynamics simulation: the Langevin piston method. *J. Chem. Phys.* **1995**, *103*, 4613−4621.
(45) Darden, T.; York, D.; Pedersen, L. Particle mesh Ewald: An NâNÉ log (N) method for Ewald sums in large systems. *J. Chem. Phys.* **1993**, *98*, 10089−10092.
(46) Bakan, A.; Meireles, L. M.; Bahar, I. ProDy: protein dynamics inferred from theory and experiments. *Bioinformatics* **2011**, *27*, 1575−1577.
(47) Bakan, A.; Bahar, I. The intrinsic dynamics of enzymes plays a dominant role in determining the structural changes induced upon

https://doi.org/10.1021/acs.jpcb.1c03982
J. Phys. Chem. B 2021, 125, 9738−9750

inhibitor binding. *Proc. Natl. Acad. Sci. U.S.A.* **2009**, *106*, 14349−14354.
(48) Lange, O. F.; Lakomek, N.-A.; Farès, C.; Schröder, G. F.; Walter, K. F. A.; Becker, S.; Meiler, J.; Grubmüller, H.; Griesinger, C.; de Groot, B. L. Recognition dynamics up to microseconds revealed from an RDC-derived ubiquitin ensemble in solution. *Science* **2008**, *320*, 1471−1475.
(49) van de Locht, M.; Donkervoort, S.; de Winter, J. M.; Conijn, S.; Begthel, L.; Kusters, B.; Mohassel, P.; Hu, Y.; Medne, L.; Quinn, C.; et al. Pathogenic variants in TNNC2 cause congenital myopathy due to an impaired force response to calcium. *J. Clin. Invest.* **2021**, *131*, No. e145700.
(50) Immadisetty, K.; Sun, B.; Kekenes-Huskey, P. M. Structural Changes beyond the EF-Hand Contribute to Apparent Calcium Binding Affinities: Insights from Parvalbumins. *J. Phys. Chem. B* **2021**, *125*, 6390.
(51) Kasuya, G.; Fujiwara, Y.; Takemoto, M.; Dohmae, N.; Nakada-Nakura, Y.; Ishitani, R.; Hattori, M.; Nureki, O. Structural insights into divalent cation modulations of ATP-gated P2X receptor channels. *Cell. Rep.* **2016**, *14*, 932−944.
(52) Immadisetty, K.; Polasa, A.; Shelton, R.; Moradi, M. Elucidating the Molecular Basis of pH Activation of an Engineered Mechanosensitive Channel. **2019**, bioRxiv:10.1101/707794.
(53) Stelzl, L. S.; Fowler, P. W.; Sansom, M. S. P.; Beckstein, O. Flexible Gates Generate Occluded Intermediates in the Transport Cycle of LacY. *J. Mol. Biol.* **2014**, *426*, 735−751.

https://doi.org/10.1021/acs.jpcb.1c03982
J. Phys. Chem. B 2021, 125, 9738−9750